Relation of Halokinesis and Associated Faulting to Subsidence and Land Loss in the Chenier Plains, Cameron Parish, Louisiana

A Thesis

Presented to the

Graduate Faculty of the

University of Louisiana at Lafayette

In Partial Fulfillment of the

Requirements for the Degree

Master of Science

Wiley M. Griffin IV

Summer 2022

Relation of Halokinesis and Associated Faulting to Subsidence and Land Loss in the Chenier Plains, Cameron Parish, Louisiana

Wiley M. Griffin IV

APPROVED:

Raphaël Gottardi, Chair
Associate Professor
Department of Geology

Davide Oppo
Assistant Professor
Department of Geology

Jorge Andres Villa-Betancur
Assistant Professor
Department of Environmental Science

William R. Finley
Instructor
Department of Geology

Mary Farmer-Kaiser
Dean of the Graduate School

Griffin IV, Wiley M. Bachelor of Science, Valdosta State University, Spring 2019; Master of Science, University of Louisiana at Lafayette, Summer 2022
Major: Geology
Title of Thesis: Relation of Halokinesis and Associated Faulting to Subsidence and Land Loss in the Chenier Plains, Cameron Parish, Louisiana
Thesis Director: Dr. Raphael Gottardi
Pages in Thesis: 51; Words in Abstract: 280

Abstract

The greatest threat to coastal Louisiana is land loss. The major contributing factor for land loss is the poorly understood process of subsidence. Subsidence, controlled by several integrated factors that exert feedback on each other, makes an unequivocal recognition of its causes challenging. This study focuses on the relationship between tectonics and land loss, specifically faulting and halokinesis. Previous studies have used surface data to show that active faults have a relationship to subsidence. However, they were focused on the Mississippi Deltaic Plain, an area strongly affected by Holocene sediment compaction associated with Mississippi River Delta deposition. This study focuses on the Chenier Plain of southwestern Louisiana, a micro-tidal coastline influenced by low energy waves, but not affected by the compaction processes of the Mississippi River. We use subsurface data to establish fault location and geometry within the study area. Expansion indices were calculated from the well logs to compare strata expansion (growth) on the hanging wall vs footwall of the faults. Growth seen in the hanging wall implies an active down slip motion along the fault leading to subsidence of the downthrown area. The subsurface investigation is compared to surface satellite imagery gathered from 1984 to 2022. The surface data shows that the area downthrown of the identified faults has subsided, and what was once occupied by marsh vegetation, is now occupied by a large water body supporting the hypothesis of

tectonically controlled land loss. Thus, the results gathered from this methodology demonstrates that deep fault activity linked to salt tectonics is a leading factor contributing to coastal subsidence land loss in all areas of coastal Louisiana, even those not subject to the influences of recent Mississippi River deposition.

Acknowledgements

I would like to thank Chris McLindon with the New Orleans Geological Society for introducing this project and offering his support through its completion. I would also like to thank Ryan Weber, president of Paleo Data Inc., for providing paleo data to this project at no cost. Thanks also to William Dore', Bill Terrell and SAI Geoconsulting Inc. for allowing me access to the seismic survey of Cameron Meadows field. Access to this survey was beneficial in producing the results. I would also like to extend an additional thanks to Bill Terrell, not only for his help in accessing the permission necessary to view this survey, but for his guidance and sharing of knowledge on Cameron Meadows field. I want to thank my thesis advisor Dr. Raphael Gottardi for his support and guidance throughout this project and its completion, as well as his guidance throughout my time in graduate school. Dr. Gottardi's support was not only beneficial to the success of this project, but to my success as a graduate student. I also want to thank Mr. William Finley for his guidance and teaching on techniques subsurface mapping. Mr. Finley has worked extensively with me throughout my graduate career in addition to this project, and his guidance and mentorship has helped me become a better geoscientist. I additionally would like to thank the other members of my thesis committee, Dr. Davide Oppo and Dr. Jorge Villa, for their support and input on this project. Last, I would like to thank my family for their continued love and support through my academic and professional career.

Table of Contents

List of Figures

List of Tables

1. Introduction

Most coastal Louisiana is experiencing rapid subsidence, and rising sea level will further exacerbate land loss. The projected cost is $3.6 billion in direct financial losses to homes, businesses, and infrastructure over the next 50 years (Barnes and Virgets, 2017). Assessing how coastal subsidence evolves is complex because the strong interdependence of the mechanisms driving subsidence hinders the univocal identification of its causative factors (e.g., Yuill et al., 2009). Most subsidence-related research in the United States has been focused on the evolution of the Mississippi River Delta (Coleman et al., 1998; Dokka, 2006; Dokka et al., 2006; González and Törnqvist, 2006; Törnqvist etal., 2006, 2008; Day et al., 2007; Meckel et al., 2007; Yuill et al., 2009; Yu et al., 2012; Wolstencroft et al., 2014; Shen et al., 2017; Chamberlain et al., 2018). This research identified six (6) parameters controlling subsidence in Louisiana: (1) faults growth and halokinesis, (2) compaction of Holocene sediments, (3) sediment loading, (4) glacial isostatic rebound, (5) withdrawal of subsurface fluid, and (6) surface water management. Although subsidence in the Mississippi Deltaic Plain is dominated by sediment compaction, little is known about how the various processes operate in other areas of the Louisiana coast, such as the Chenier Plain. The Chenier Plain contrasts the Mississippi Deltaic Plain by its lack of influence from Holocene sediment loading and compaction. The Pleistocene Formation lies approximately 33 ft below the land surface in the Chenier Plain, compared to the 984 ft in the Mississippi River Delta (Kulp, 2000; O'Leary and Gottardi, 2018). The Chenier Plains are experiencing a high subsidence rate of ~8.9 mm/year (Figure 1 & 2; Nienhuis et al., 2017)

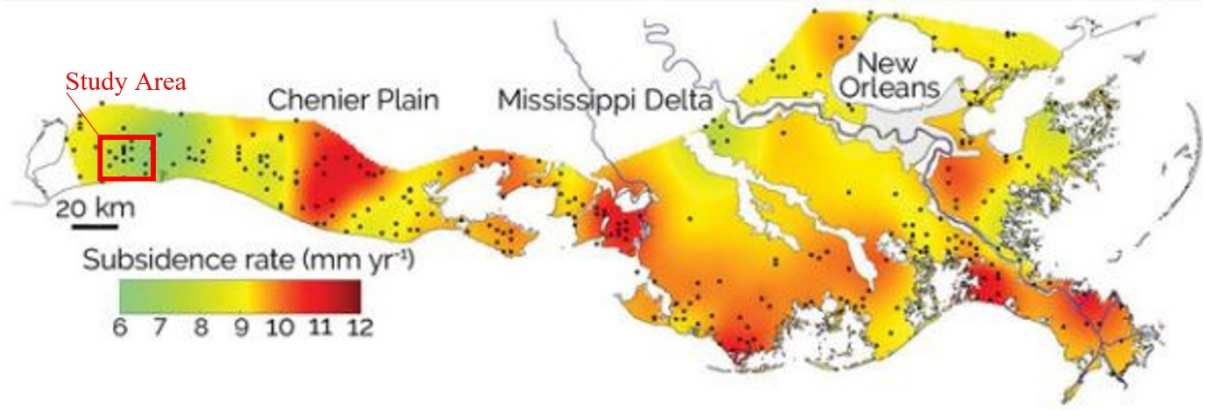

Figure 1: Map showing subsidence rates in coastal Louisiana modified from Nienhuis et al. (2017). Black dots are surface elevation tables installed after Hurricane Katrina in 2005. Red box identifies study area for this project.

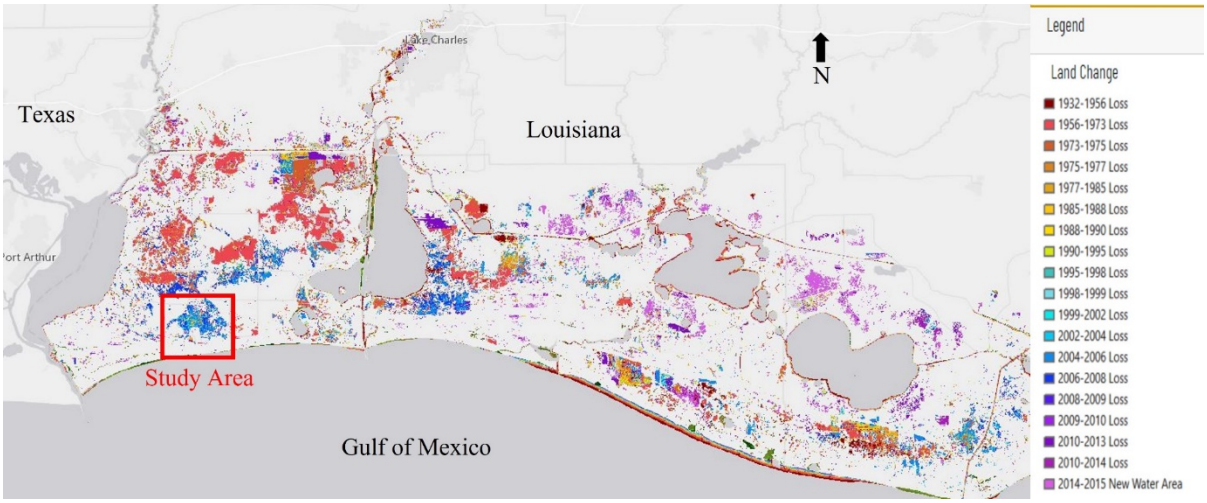

Figure 2: Map illustrating land change in costal Louisiana and location of the study area, Cameron Meadows Field (red box). The color bar denotes the time period in which land change occurred (modified from Couvillion et al., 2017).

As part of a broader research initiative started by the New Orleans Geological Society, this study aims at investigating the investigating the halokinetic faulting relationship to surface subsidence and its impact on coastal Louisiana land. The northern margin of the Gulf of Mexico is littered with extensional faults. Extensive subsurface well data, seismic,

and LIDAR have been used in recent studies to show a relationship between active faulting and subsidence. Gagliano et al. (2003) established and evaluated the relationship of faults to local and regional land loss. In the Golden Meadows Fault Zone in SE Louisiana, it has been demonstrated, using arial imagery, geoarchaeological data, tide gauge records and measurements from re-leveled benchmarks, that small increments of vertical displacement along faults result in large areas of submergence and land loss particularly in low-lying coastal areas (Gagliano et al., 2003). Displacement along these faults has been a fundamental geologic control on the geomorphic evolution of coastal Louisiana as evidenced by subsurface stratigraphic relationships (Culpepper, 2019).

Most of this subsidence and land loss research, including Gagliano et al. (2003) has been in the Mississippi Deltaic Plain under the dominant influence of Holocene sediment compaction. Currently, regional subsidence due to faulting and/or salt movement has been under-recognized. Furthermore, much of this research has been limited to surface or shallow subsurface data. Deep fault activity and its slip rate related to subsidence has been ignored. By investigating an area where subsidence is largely due to tectonics, a better understanding of how fault processes have controlled land loss can be ascertained.

This study will focus on faults identified in the Chenier Plain of Southwest Louisiana, outside the influence of the extensive Holocene sediment compaction in the Mississippi Deltaic Plain. The deep-seated component of fault activity will be investigated for its relationship to subsidence and land loss. The hypothesis is halokinetic fault activity is a controlling factor to subsidence and land loss in coastal Louisiana areas that are not influenced by the Mississippi Deltaic Plain.

Cameron Parish is located in the southwest corner of Louisiana bordered by Texas to the west, Calcasieu Parish to the north, Vermillion Parish to the east, and the Gulf of Mexico to the south. The area of study focuses on a known salt dome in an active oil field listed as Cameron Meadows (Figure 3). Cameron Meadows is west of Calcasieu Lake, approximately 8 km north of the Gulf Coast and 27 km east of the Texas state line. Cameron Meadows is located in a geological region known as the Chenier Plain (Figure 3). Cheniers are discussed in detail in Section 2.3.

Aerial photographs of Cameron Meadows show suspected surface expressions of faults bounding the location of the known salt dome. The surface expression of the suspected faults is delineated by comparing aerial photographs of different time periods. Through time, changes in marsh vegetation and water appear on the down thrown blocks of the suspected faults. Gagliano et al. (2003) notes a verified correlation of the signature of fault surface expressions and proven subsurface faults. In coastal Louisiana, surface expressions of faults are characteristically arc-shaped lineaments up to five miles in length with associated land loss on the down thrown block (Gagliano et al. 2003). This observation is not limited to Gagliano et al. (2003). A more recent study by UL Lafayette MS student O'Leary in 2018 was conducted in the Chenier Plain of Cameron Parish, Louisiana. O'Leary (2018) confirmed though seismic and well log data a correlation of the faults mapped in the subsurface and their surface expression in aerial photos. The down thrown blocks of the studied faults were occupied by water bodies and had experienced land loss (O'Leary, 2018).

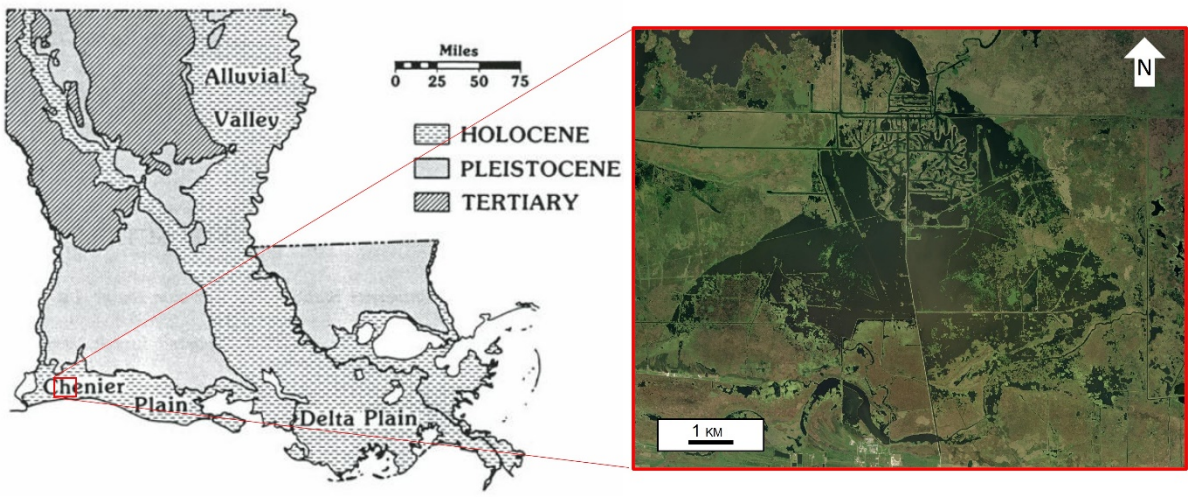

Figure 3: Location of study area modified from Penland and Suter (1989), showing Chenier Plain and zoomed in satellite image of study area.

2. Regional Geology

2.1. Gulf of Mexico

The Gulf of Mexico Basin was formed during the Mesozoic by the rifting of the North American, South American and African plates. This rifting event established the fundamental structural and stratigraphic framework of the basin. This includes the deposition of the Jurassic Louann Salt and overlying formations that eventually resulted in the lateral flow of the Louann salt, as well as the vast regime of extensional faults that bound the subsided graben.

The formation of the Gulf of Mexico begins with the breakup of Pangea in the Late Triassic. The rifting produced a subsiding graben bounded by large, regional, normal faults. Dating of sedimentary sequences, including red-beds and predominantly nonmarine sediments, suggest the first tectonic phase of rifting lasted from Late Triassic through Middle Jurassic and was characterized by extensional deformation that resulted in active grabens (Salvador, 1987). Stretching of the basin continued through the early part of the Late Jurassic as the Yucatan platform drifted south (Salvador, 1987). This resulted of the lateral flow of the Louann Salt toward the center of the newly formed basement (Hudec et al., 2013). By the Early Cretaceous, tensional deformation had ceased as the Yucatan Platform had drifted to its present position.

The second tectonic phase occurs toward the end of the Late Jurassic as crustal stretching came to a halt and the vertical tectonic subsidence of the basin begins. This further assisted in the lateral flow of salt toward the center of the basin. (Salvador, 1987; Hudec et al., 2013). The basic structural, and geographic features of the Gulf of Mexico were, for the most part in place by the end of the Jurassic. However, vertical tectonic activity, driven by

gravitational forces, has continued since the end of the Jurassic, resulting in basin subsidence and salt deformation (Salvador, 1987; Wu et al., 1990). The Gulf of Mexico is the most active passive margin in North America and is characterized by active subsidence (Russel and Howe, 1935).

2.2. Halokinesis and Faulting Process

Halokinesis, or salt tectonics, is the movement of salt and salt bodies. The thick deposits of salt that form domes and diapirs are restricted to the margins of the Gulf of Mexico, which includes coastal Louisiana (Antoine and Bryant, 1969). Evaporite deposition is poorly dated. However, the ages of the underlying and overlying sedimentary units, as well as igneous intrusions, suggest that salt deposition occurred in the later Middle Jurassic (Hudec et al.; 2013, Pindell et al., 2020). This includes the Louann Salt deposited on the north bank of the Gulf of Mexico. While the original thickness of salt deposited may be speculative at 3-4 km in the deepest part of the basin, the large quantity of salt deposited suggests a period of active graben subsidence during the first tectonic phase of extensional deformation (Salvador, 1987; Hudec et al., 2013). Sea floor spreading occurs in the Late Jurassic as the Yucatan drifts south, and gravity sediment loading initiates the lateral flow and deformation of salt toward the center of the newly formed basement (Salvador, 1987; Hudec et al., 2013). As stated previously, vertical tectonic subsidence occurring after the cessation of crustal stretching, further assisted in the basin-ward flow of the Louann Salt (Salvador, 1987). Increase in sediment loading throughout the Cretaceous and Paleogene remobilized the Louann Salt. Through the Paleogene, the rapid deposition of sediment from the progradation of the shelf margin had induced down-slope spreading of autochthonous salt. The increase in sediment load results in salt swells, domes and anticlines. This assists in the upward movement of salt

and diapirism which lasted through the Pleistocene (Wu et *al.*, 1990). Allochthonous salt tongues emplaced in stratigraphically younger sediments will spread down-slope with the compacted sediments. As the burial depth and compaction increases, an inverse in density between the salt and overlying strata occurs causing the salt to overthrust and climb upward in order to maintain dynamic equilibrium (Wu et al., 1990). This plastic flowage of salt uplift, folds, and faults the Mesozoic and Cenozoic strata. Fault systems created by salt movement include large, down to the basin growth faults, as well as smaller normal faults that are localized around salt domes.

The most common type of fault associated with halokinesis in coastal Louisiana, is the roller fault (Rowan et al., 1999). A roller fault is a listric growth fault that is dominantly basinward dipping and soled into a salt layer or dome (Rowan et al., 1999). As with other growth faults, the hanging wall generally contains expanded growth sections that are tilted toward the fault. Roller faults can be found in numerous different settings involving autochthonous or allochthonous salt structures. More applicable to this study would be faults associated with bulb-shaped salt stocks, or domes and diapirs. Where salt domes are found, the roller faults are atypical in the sense that the dip of the fault is not necessarily basinward. The fault could essentially dip in all directions above the dome. Their classification as a roller fault is due to the similar geometric relationship of the fault and top of salt, as well as the hanging wall and footwall (Rowan et al., 1999). An important note is roller faults accommodate gravity spreading or gliding of the overburden strata along the salt detachment (Rowan et al., 1999). However, roller faults associated with bulb-shaped salt stocks tend to only be found directly above the salt stock. With the confining geometry of the salt dome, lateral translation downslope is minimal, and the roller faults tend to die out upward (Rowan

et al., 1999). While the roller fault sub-type may be the most common, and certainly found in this author's study area, another sub-type of normal fault may be more applicable: ramp faults. A ramp fault is a slightly listric growth fault formed as a salt ramp, or bulb, cuts up section in the direction of salt emplacement (Rowan et al., 1999). Ramp faults are found on the up-dip margin of bulb-shaped salt stocks. The ramp fault is highly arcuate, and the strike can curve up to 180° following the perimeter of the dome. These faults are characteristic in their arcuate shape at the surface, and the faults always dip down into the up-dip margins of the salt dome (Rowan et al., 1999).

2.3. Chenier Plain

The Chenier Plain is the geological region that encompasses the coast of Southwest Louisiana, west of the region known as the Mississippi Deltaic Plain (Figure 3). The Chenier Plain is characterized by its long, wooded beach ridges. These ridges are known as cheniers, a word derived from Cajun French meaning live oak. The ridges are known to be well drained and fertile giving habitat to healthy vegetational cover that includes large live oaks (Russel and Howe, 1935). This region is currently subject to high subsidence rates and sea-level rise (Nienhuis et al., 2017). While the coastal area is classified as microtidal with low wave energy, this region is influenced by increased wave energy and mud transport yearly during hurricane season and other major storms (Owen, 2008). The area intervening the cheniers consists of marsh and mudflats (Owen, 2008). The Chenier Plain was formed by the natural alteration of the Mississippi River and from wave action during shoreline retreat (Figure 4; Russel and Howe, 1935; Owen, 2008). As the Mississippi River altered course, the shifting delta lobes that moved westward deposited sands, fine sands and mud (Figure 4). The fast rate of the progradation impedes the removal of the fines. As the delta lobe switched

eastward, the mudflats that had been previously deposited would be reworked by wave action during shoreline retreat. The fines are worked out during this process being transported offshore, and the leftover coarser sands build the ridges that are the cheniers (Russel and Howe, 1935; Hoyt, 1969; Owen, 2008). The Chenier Plain is actively subsiding at an approximate rate of 0.35 inches per year (Gottardi and O'Leary, 2020; Nienhuis et al., 2017). The high subsidence rate is major factor in sea-level rise and shore-line erosion, despite the low wave energy (Owen, 2008). The factors which influence that subsidence will be studied in this paper.

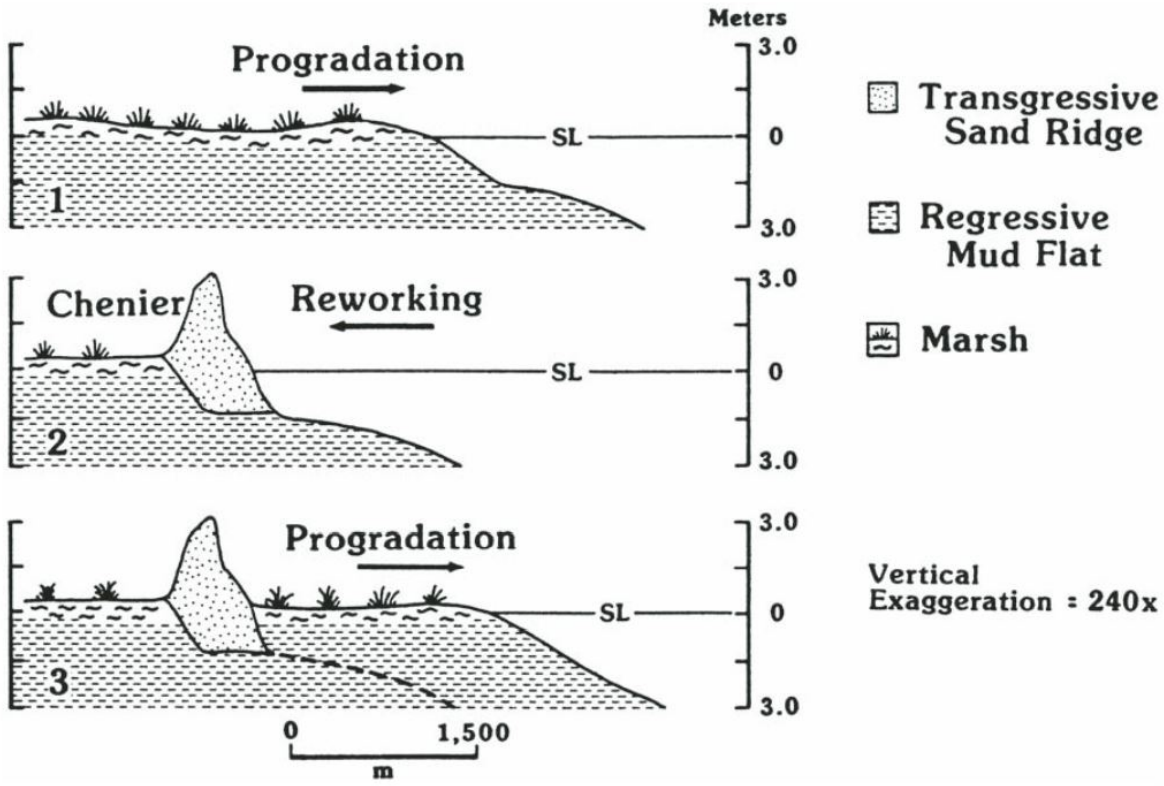

Figure 4: Hoyt's process model for the creation of the cheniers found in Chenier plain (from Owen, 2008).

3. Methods

This study uses a combination of subsurface and surface data. Subsurface data was collected using well logs downloaded from the Strategic Online Natural Resources Information System (SONRIS) website. The author was also granted permission to view a 3D seismic survey of the study area owned by William Dore' and accessed by SAI Geoconsulting, Inc. While the rights to the seismic survey were restricted, permission to extract subsurface data from fault surfaces was granted. Subsurface paleo data was provided by Paleo-Data Inc. to correlate stratigraphic age. . Surface data from aerial photographs was collected from SONRIS and Google Earth time lapse software.

A total of 274 wells completed between 1936 and 1999 were downloaded from SONRIS and imported into IHS Kingdom Suites subsurface mapping software (Figure 5). Out of the 274 wells, raster images of electric logs containing resistivity and spontaneous potential for 84 wells were imported. Wells not included either had no electric logs available or were of poor quality. Logs with a minimum depth of 6000 ft were used excluding the wells located at the crest of the salt. Electric logs were correlated to identify fault depth and displacement for mapping fault surfaces following standard techniques of subsurface geologic mapping (Tearpock and Bischke, 1991).

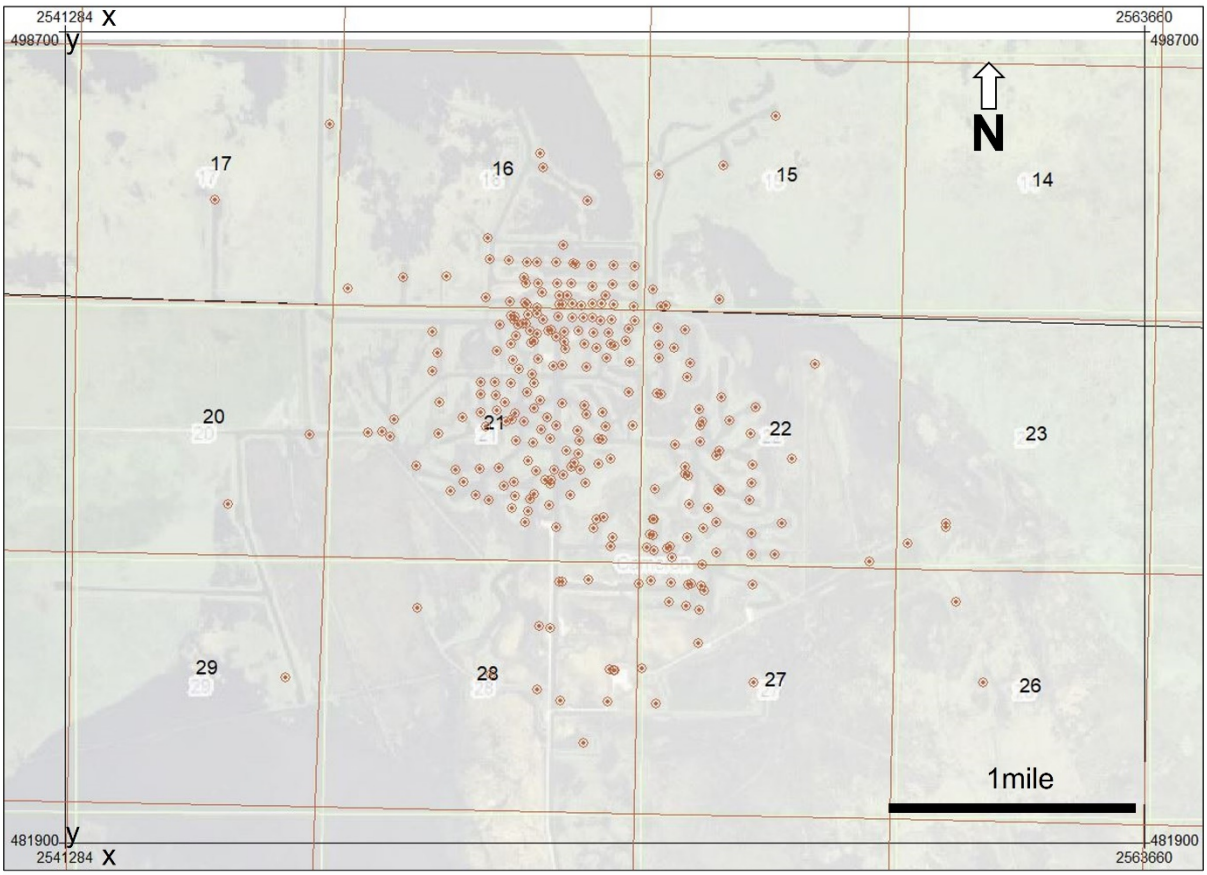

Figure 5: Base map exported from IHS Kingdom Suites mapping software, illustrating well locations in the study area. A satellite image of the study area captured in 2008, imported from SONRIS, is added as a culture file to the base map.

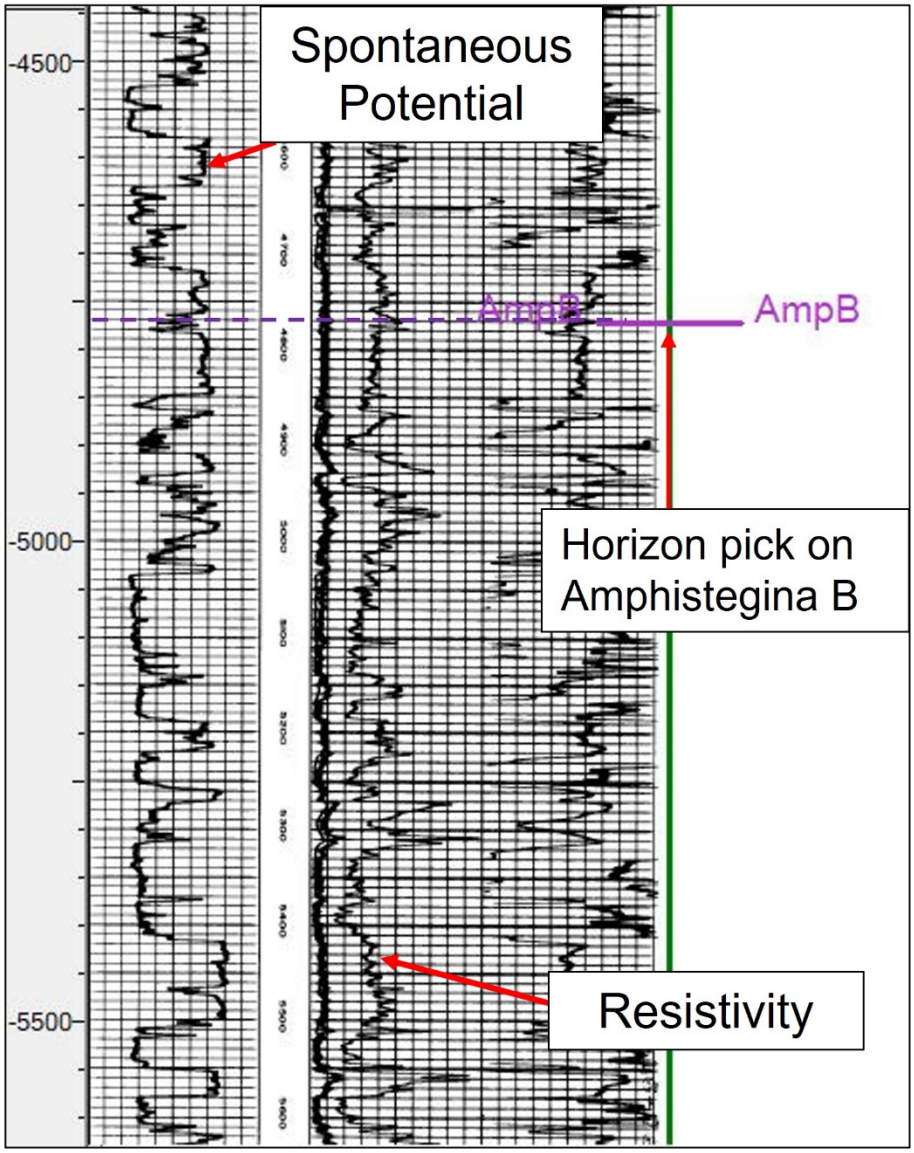

Figure 6: Section of electric well log used in data set imported from SONRIS. Spontaneous potential and resistivity, highlighted here by red arrows, are used to identify sequences of sand and shale. Sequences that are easily identifiable are picked in the section and correlated across other well logs in the study area by identifying the same sequence. An example of a horizon pick can be seen here on the Amp B, which is located on an easy identifiable shale break found across the study area. Correlation of stratigraphic sequences are used to locate fault cuts by identifying missing section in sequence.

A structure map of Cameron Meadows Field, including a "top of salt" map both constructed by Sun Oil Company in 1962 was used as reference in this project because only one well used in this study showed indication of reaching the top of salt. As stated previously, access to view a 3D seismic survey over the study area was granted, and it was determined that Sun

Oil's interpretation of the top of salt was sufficient to be used in this study. The Middle Miocene paleomarker, Amphistegina B, was a noticeable shale log signature around the -5000 ft depth (Figure 6). This shale marker was used to correlate the well logs and map structure over the top of salt. Other correlations were made using identifiable shale breaks between depths of -2000 ft and -6000 ft. Fault cuts were identified by missing sections in the correlated well logs. The area around the salt dome is littered with antithetic and synthetic faults that form a map view radial pattern around the dome. Primary focus was given to the large faults that bound the perimeter of the dome that seem to have the most control on subsidence. To assist in this focus, an aerial image from 2008 was imported into the base map from SONRIS. The suspected fault trace of the main fault can be identified by its highly arcuate shape with a water body located in the down-thrown side toward the salt dome. Using the trace as 'zero' contour in subsurface elevation, an estimated constant dip of 60° was used to calculate the map contour spacing between 1000 ft contours.

$$\frac{1000ft\ elevation}{\tan(60)\ dip\ angle} = 577ft\ contour\ spacing$$

Contours created from the aerial image and estimated dip served only as a guide to determine areas of emphasis when attempting to locate fault cuts and establish a true fault surface. Once fault cuts were identified, the contours of the true fault surface were adjusted and more accurately mapped.

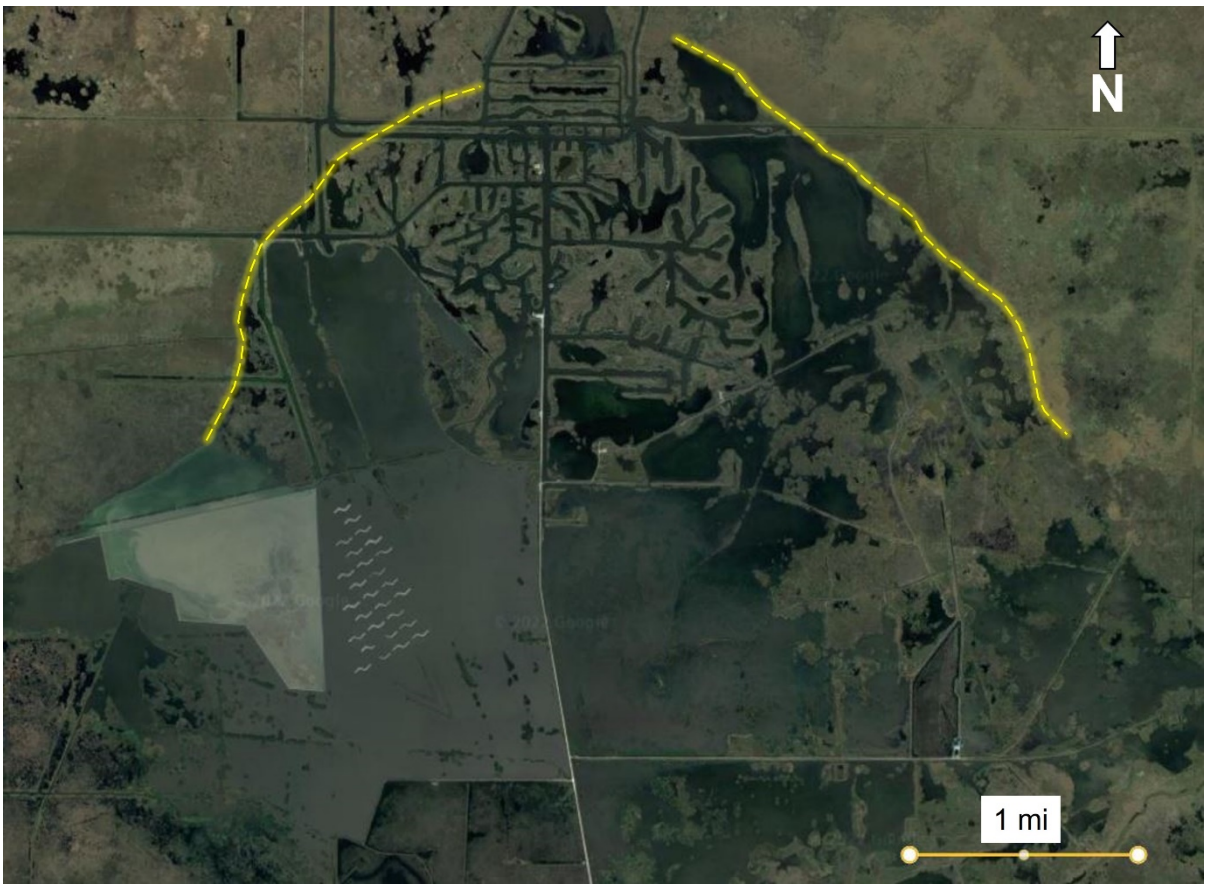

Figure 7: Modified 2022 satellite image from Google Earth showing the Cameron Meadows field study area. Fault traces are highlighted in yellow dashed lines.

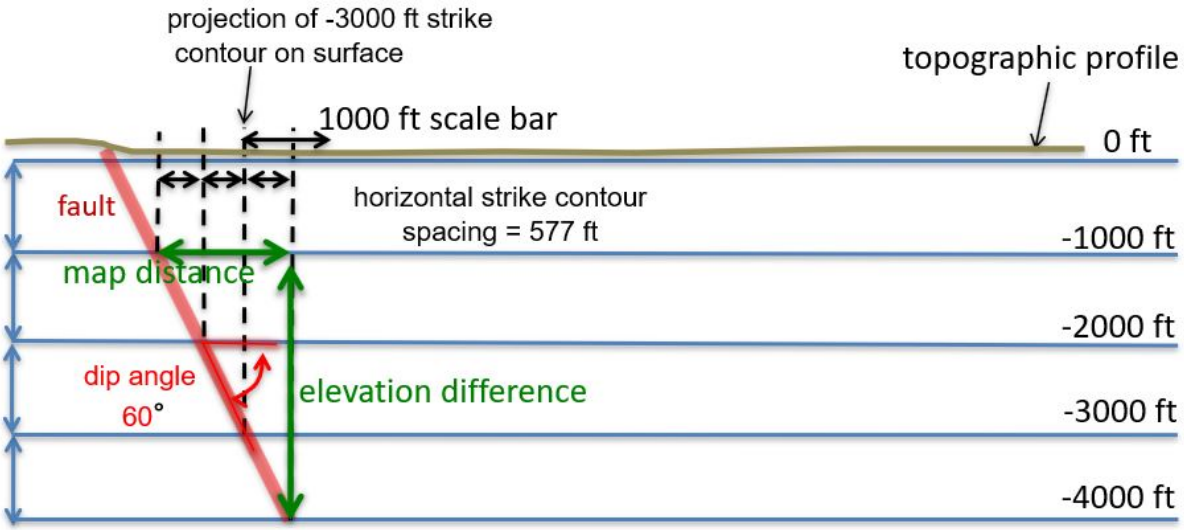

Figure 8: Graphic showing how an artificial fault surface was created using the fault trace as 0ft contour elevation and estimating a dip. Due to data quality and the vast expanse of faults in the area, this method of using an artificial fault surface helps by highlighting areas of the well log that should intersect the investigated fault.

To better confirm the accuracy of the created fault surfaces, the author was given access to a 3D seismic survey of the study area. Permission was given for the author to map the fault surface in time. Crosslines running west to east perpendicular to the fault surface, were used with 10 traces per skip. Faults were picked from visible offsets of seismic reflectors observed near surface down to where they truncated the top of salt. Faults were extrapolated to the surface using a constant dip from the nearest visible offset. A contour map of the fault surface was created in time from the picked intervals and exported. Due to incompatibilities with different software versions of IHS Kingdom, the contours created in time were not able to be imported. Instead, the file was converted to a .tif image and successfully imported as a culture file. Contours created with seismic data were compared to those created in depth logs as well as the aerial image and were found to be consistent with this author's interpretation. The extrapolated point where the fault breaches the surface in time matched well with the fault trace seen in the aerial photograph. By combining the seismic data with well log data, a more accurate interpretation of the fault surfaces was generated.

Surface data from aerial images downloaded from SONRIS and Google Earth are used in this study. A timelapse of photographs taken from 1980 to present, highlight areas experiencing land-loss. The subsidence of these areas is recognized by water bodies occupying what was once marsh. As described by Gagliano et al. (2003) and Dokka (2006), characteristics of subsidence due to faulting include the die-back and browning of marsh vegetation with a water body occupying the down-thrown block of the fault. These characteristics of tectonic subsidence are gathered from the surface data and used to identify the surface expression of the main fault.

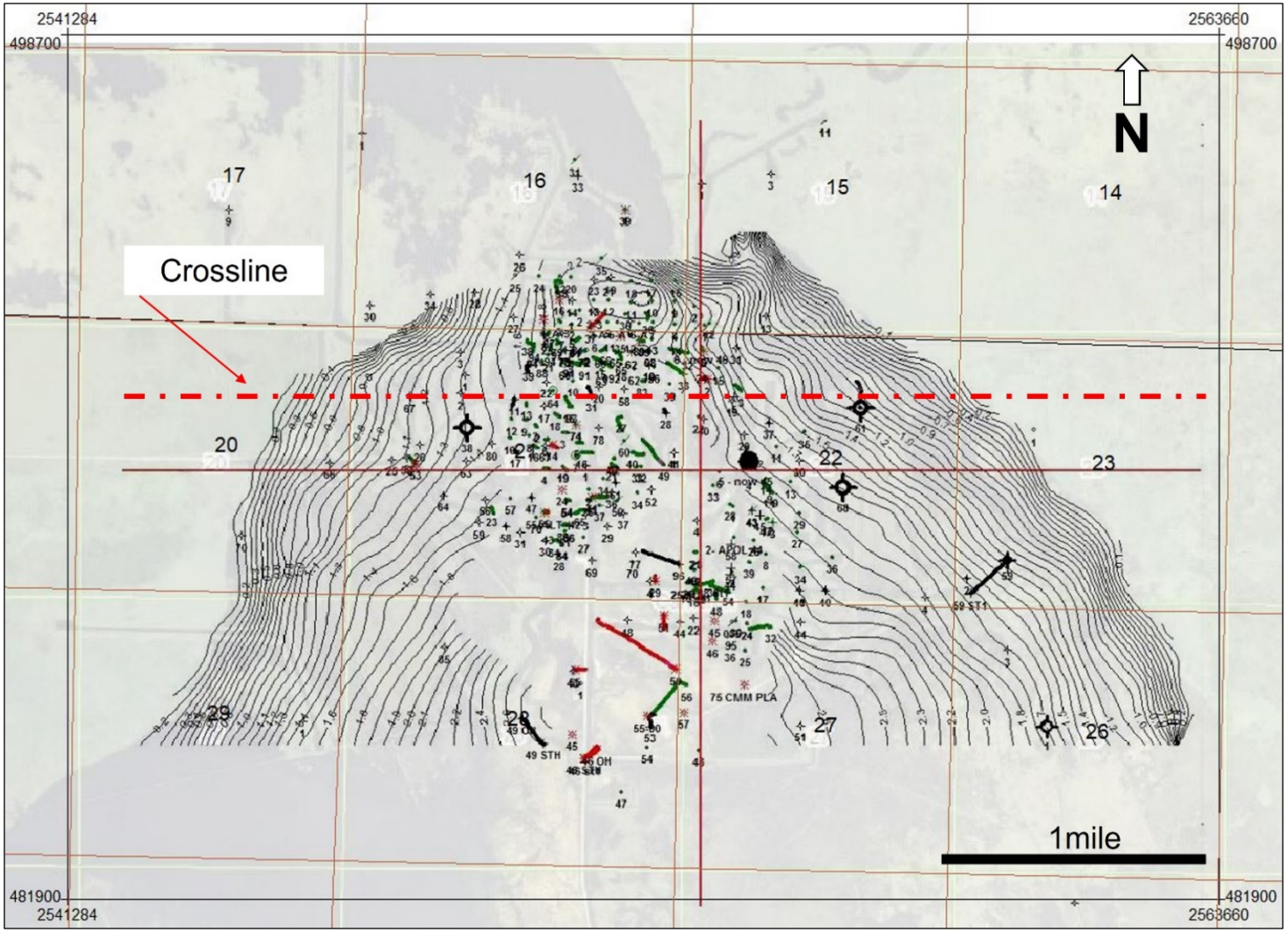

Figure 9: Fault surfaces mapped in time from a 3D seismic survey over the study area. This data was accessed through SAI Geoconsulting with permission from the owner, William Dore'. This map was exported from the 3D seismic survey and compared to the data findings in this study. The fault surfaces picked in seismic were picked as high as data quality would allow. The fault surface is lost in shallow sections due to near surface seismic noise. The fault surface was extrapolated to the surface using constant dip. The dashed red line is the crossline depicted in Figure 10.

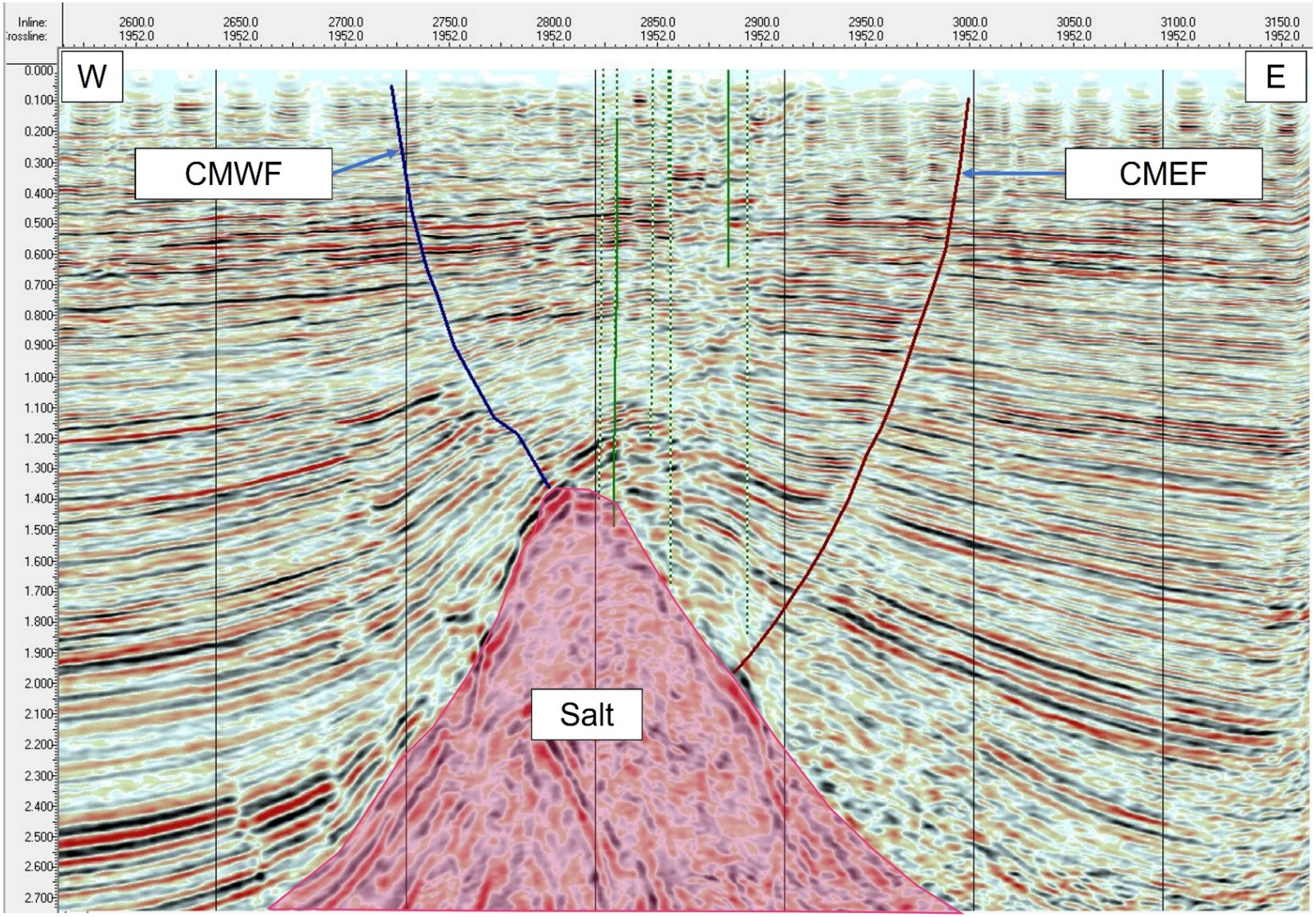

Figure 10: Screen grab of crossline slice in 3D seismic survey taken at SAI Geoconsulting office. Figure shows CMWF and CMEF, mapped by the author, truncating the salt and breaching the surface. Crossline location is shown in Figure 9.

4. Results

4.1. Characterization of Faults

Satellite images acquired from the SONRIS database were used to interpret the surface expression of primary faults based on characteristics previously mentioned. The author used of the term primary fault to indicate those faults most likely associated with activity leading to subsidence. Two primary faults identified are: Cameron Meadows West Fault (CMWF) and Cameron Meadows East Fault (CMEF) (Figure 11). CMWF bounds the known salt dome to the west with a NE strike dipping to the SE. CMEF bounds the salt dome to the east and strikes NW dipping to the SW. Twenty-six electric well logs, variously located on the upthrown and downthrown sides of these faults, were correlated to identify fault depth and displacement data used to map the fault surfaces. The correlations were made on identifiable patterns of shale and sand sequences. The Amphistegina B (Amp B) paleomarker correlation was made across the field based on an Amp B shale break of Middle Miocene age found at depths ranging from -4000 ft to -5600 ft. This depth range is attributed to faulting associated with the emplacement of salt. Other correlations were made above and below the Amp B, from -2000 ft to -7000 ft, with most being consistent across the field, but some correlations were only consistent in the area adjacent to the faults. Fault cuts were identified at depth by missing sections of sand and/or shale sequences. Two fault surfaces were mapped based on the fault cuts correlated in the wells.

Ten fault cuts were identified in wells from depths of -3977 ft to -5552 ft on the downthrown block of the CMWF. No shallower faults cuts were possible due to lack of well log data. One fault cut at a depth of -4605 ft for example was imported from Sun Oil's 1962 interpretation map as no well log is available for this well. The CMWF fault surface map was

projected to the surface by the author using the extrapolated fault surface interpreted from the 3D seismic survey owned by William Dore' and SAI Geoconsulting. Results from integrating the wells fault cuts data with the seismic survey fault surface map strongly suggests the CMWF is a high angle, listric, normal fault that breaches the land surface and truncates at depth against the top of salt. The surface expression of the CMWF observed in aerial images is thus correlated to be an accurate representation of the fault surface strike where land surface breach occurs. CMWF becomes more listric (dip decreases) starting as shallow as -3000 ft. The change in dip angle is heavily influenced by the top of salt.

Five fault cuts for the CMEF were identified from -2950 ft to -6054 ft. The author's fault surface interpretation from the seismic survey guided construction of the fault surface map in depth. Results from this integration for the CMEF show, similar to the CMEF, a high angle, listric, normal fault that breaches the surface and truncates against the top of salt. The surface expression of the CMEF observed in aerial images is also found to be an accurate representation of this fault's surface breach. The CMEF is listric, but not to the degree of the CMWF. Both the CMWF and CMEF are high angle normal faults that form a graben over the top of the salt dome. Both faults dip toward the salt dome, truncating at the salt surface but also breach the land surface with a distinct surface expression.

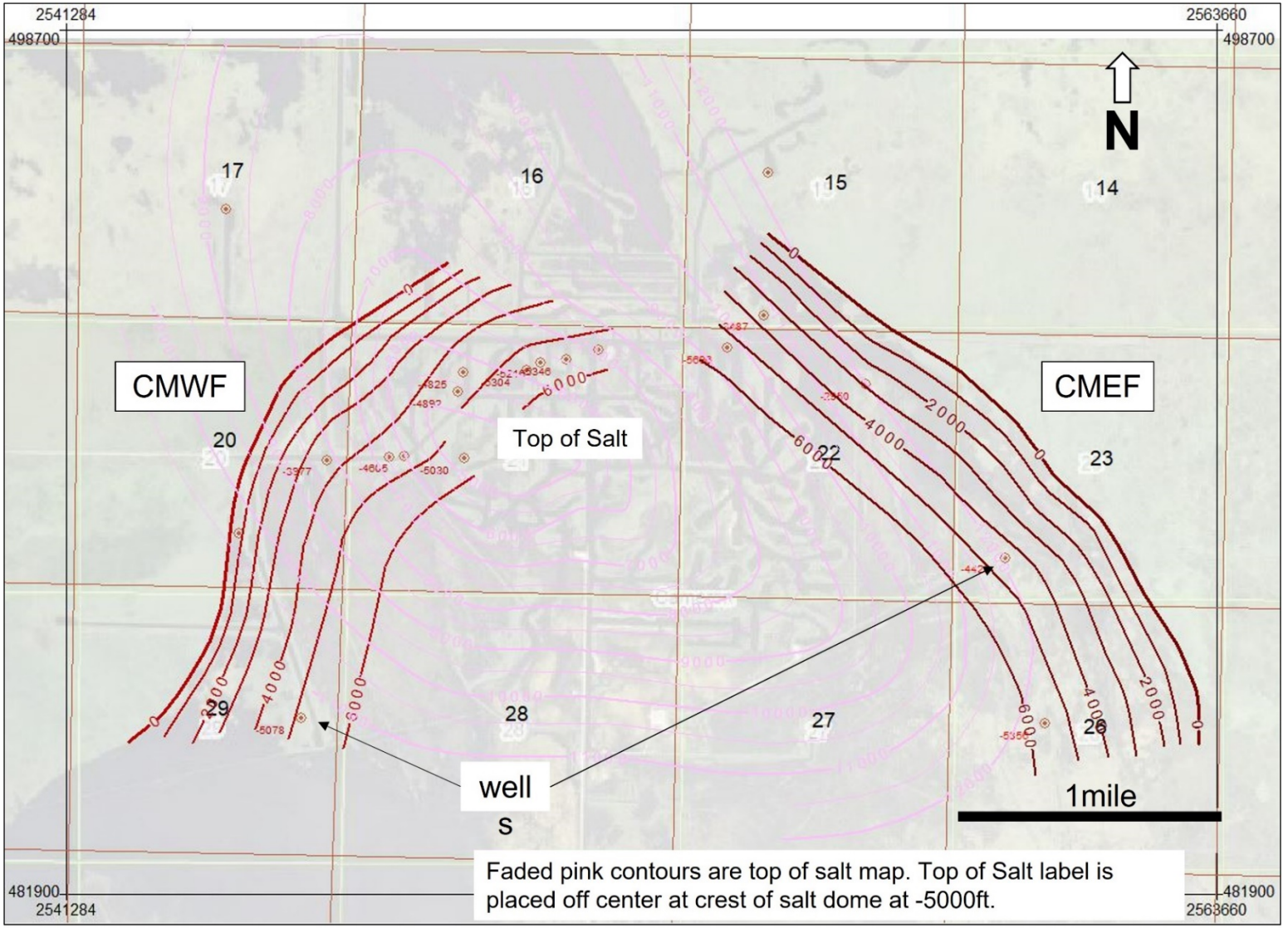

Figure 11: Base map showing top of salt mapped with 500 ft contour intervals, and two mapped fault surfaces of CMWF and CMEF, mapped with 1000 ft contour intervals. Base map is overlain on satellite image of study area imported from SONRIS. Wells used to map fault surface are shown on map.

4.2. Expansion Index

To show growth along the faults, a thickness ratio was calculated comparing interval thickness in upthrown versus downthrown wells. Multiple correlation horizons consisting of several sand and shale sequences were picked in wells located on the upthrown and downthrown sides of the fault (Figures 12-14). The depth difference between correlation horizons were calculated as the interval thickness. For example, two horizons, H1 and H2 the depth of H2 is subtracted by the depth of H1 in each well log (Figure 13). The result yields an interval thickness. The interval thickness calculated between two horizons on the upthrown block was compared to the interval thickness calculated on the same horizons on the downthrown block. Dividing the interval thickness of the downthrown block by the interval thickness of the upthrown block gives the expansion index for that horizon interval. An expansion index greater than one implies stratigraphic thickening in the hanging wall.

$$Expansion\ I = \frac{(Downthrown\ H2\ depth - Downthrown\ H1\ depth)}{(Upthrown\ H2\ depth - Upthrown\ H1\ depth)}$$

Growth in the hanging wall is observed in both faults (Figures 12-14, Tables 1 & 2). Growth is more prevalent at deeper levels and closer to the fault cut. The shallower interval in the section 29 well, located on the hanging wall of the CMWF, showed no growth. Likewise, the well in section 26, located on the CMEF's hanging wall, showed no growth. Both measured intervals are approximately 1500 ft above the fault cut found in the well.

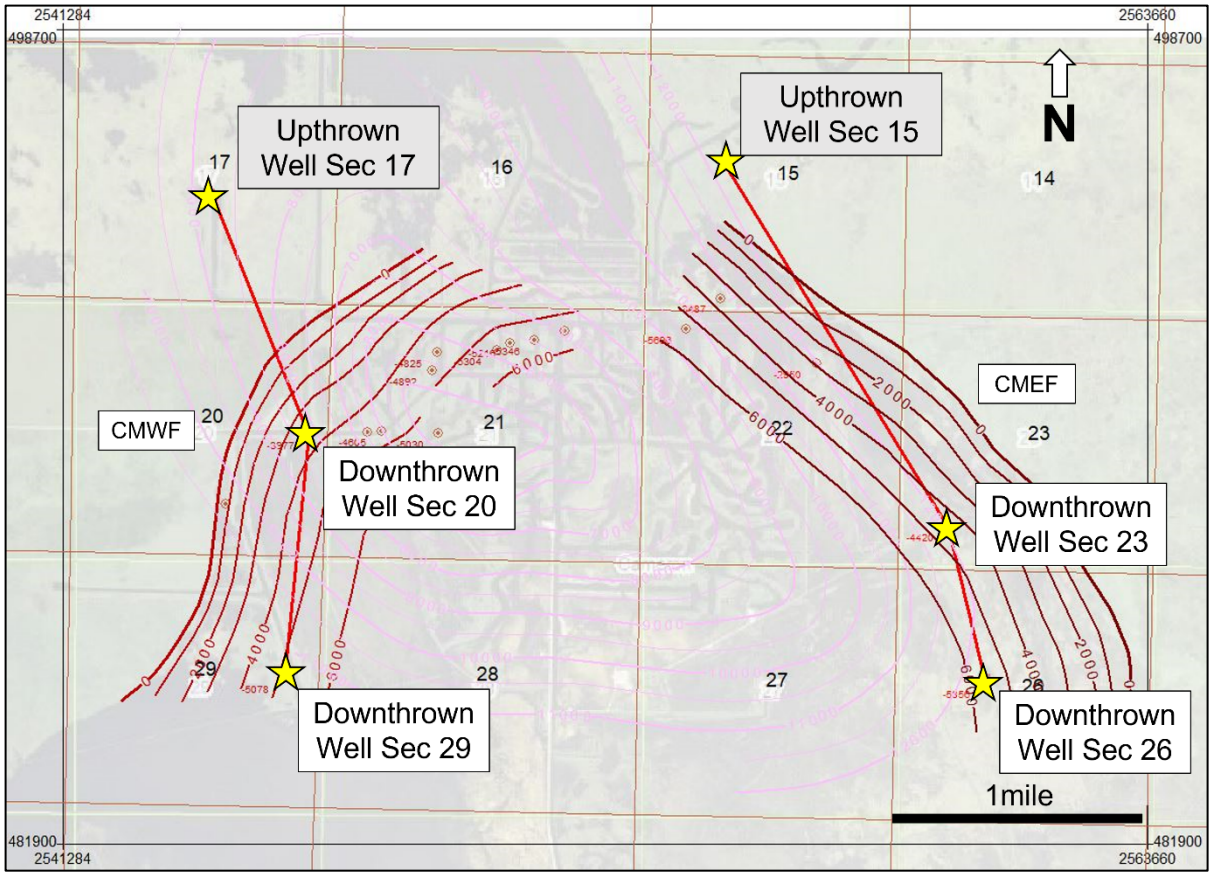

Figure 12: A red line shows a correlation line through selected wells used to calculate an expansion index. Downthrown wells were chosen based on quality of log data least impacted by salt placement.

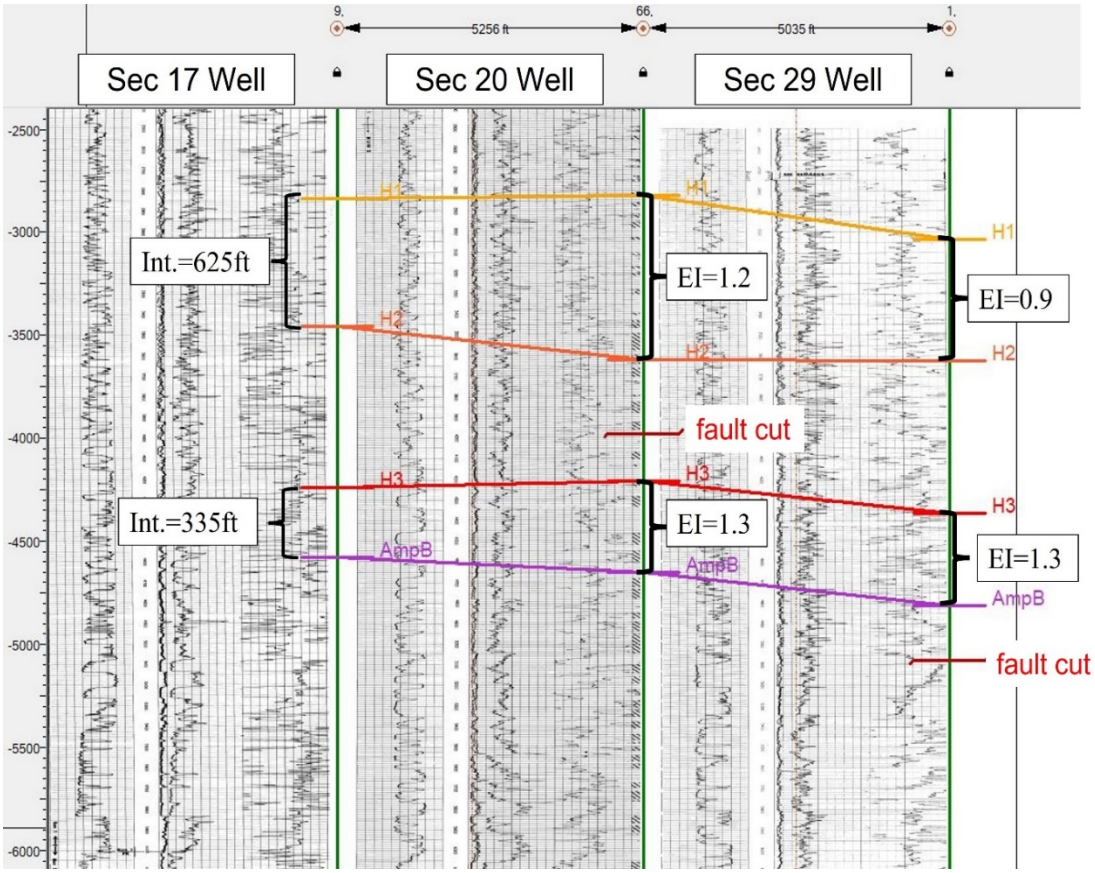

Figure 13: Correlated well logs across CMWF showing expansion index.

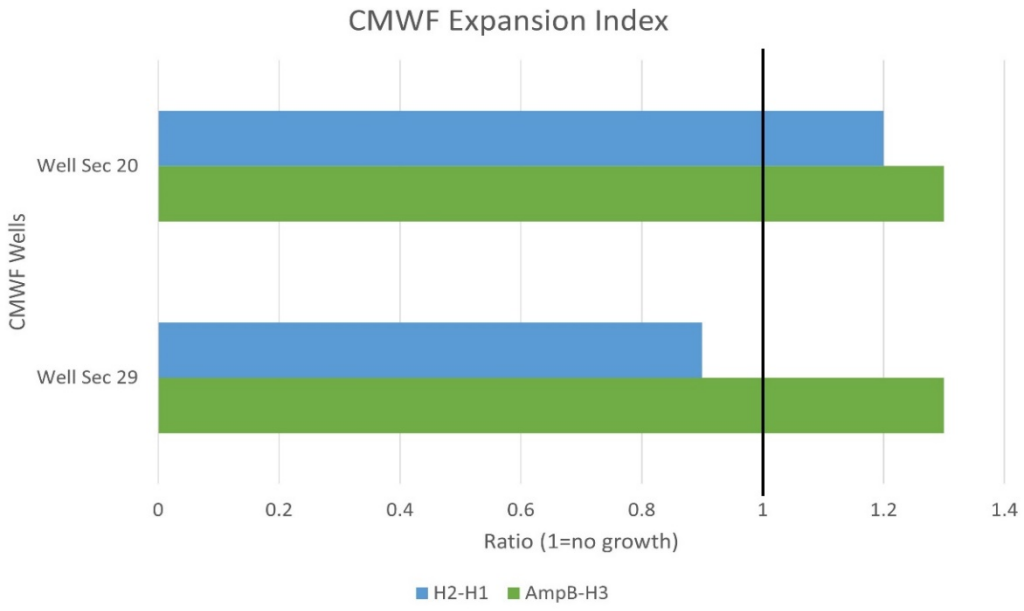

Figure 14: Graph of expansion index in downthrown wells for CMWF.

Table 1: Depths of correlated horizons picked across wells.

Horizons (Depth)		Fault					
		CMWF			CMEF		
		Upthrown Well Sec 17	Downthrown Well Sec 20	Downthrown Well Sec 29	Upthrown Well Sec 15	Downthrown Well Sec 23	Downthrown Well Sec 26
	H1	2834 ft	2822 ft	3036 ft	3278 ft	3558 ft	3524 ft
	H2	3459 ft	3618 ft	3621 ft	3913 ft	4283 ft	4182 ft
	H3	4240 ft	4205 ft	4365 ft	4462 ft	4749 ft	4819 ft
Amp B (CMWF)H4	H4	4575 ft	4648 ft	4812 ft	5006 ft	5423 ft	5678 ft

Table 2: Expansion index in downthrown wells.

Horizons		Expansion Index			
		CMWF		CMEF	
		Downthrown Well Sec 20	Downthrown Well Sec 29	Downthrown Well Sec 23	Downthrown Well Sec 26
	H2-H1	1.2	0.9	1.1	1
Amp B (CMWF)H4	H4-H3	1.3	1.3	1.2	1.5

4.3. Surface Data

Thirteen Google Earth yearly satellite images spanning from 1985 to 2022, show a progressive change through time of the landscape in the Cameron Meadows Field study area (Figures 15-18). The 1985 image shows the entirety of the study area being covered with marsh vegetation (Figure 15). As early as 1986, a variation in color between marsh vegetation on the upthrown and downthrown sides of the faults is observed. This "browning" of marsh vegetation on the downthrown side is consistent with findings of land loss observed at other faults in coastal Louisiana (Gagliano *et al*., 2003). By 1997, water begins to hold on the downthrown side as marsh begins to die back toward the surface expression of the faults (Figure 16). This continues to 2005 (Figure 17). From 2005 to 2010, land loss is rapid, and by 2010 the area downthrown is occupied by a large water body (Figure 18). The Louisiana

Coastwide Reference Monitoring System (CRMS), using land change data from USGS and Couvillion (2017), shows most of this land change occurring from 1999-2009. The immediate change from land to water, showing an arcuate shape, is the surface expression of the two faults discussed above, CMWF and CMEF. This surface expression matches the fault data collected in the subsurface.

Figure 15: Satellite image of study area modified from Google Earth captured in 1985. Study area is covered in lush marsh vegetation. A slight variation in color can be observed on the CMWF trace.

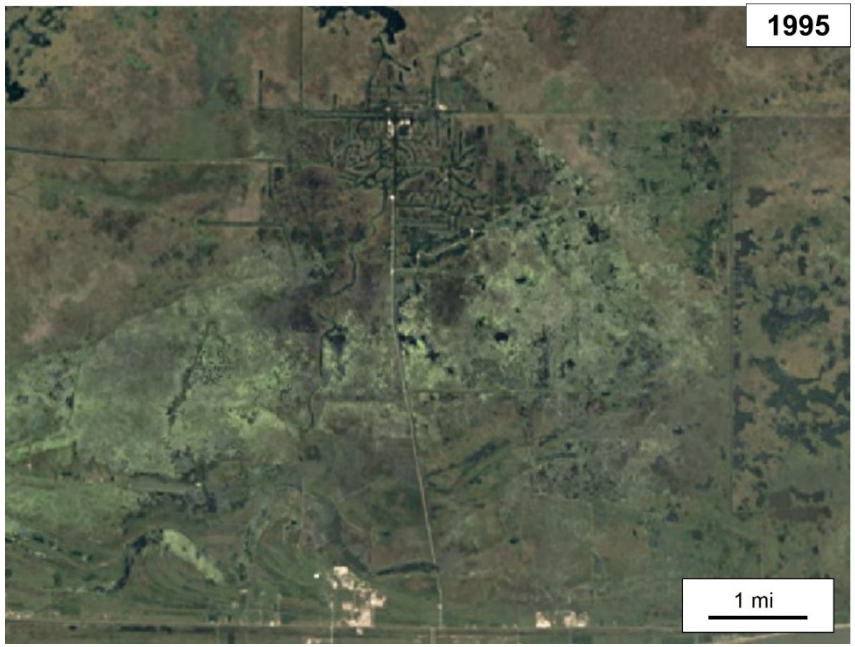

Figure 16: Satellite image of study area modified from Google Earth captured in 1995. Marsh vegetation still occupies the downthrown side of the faults. A distinct color change can be observed on the downthrown side. However, the browning of the marsh that typically occurs on the downthrown side is not seen here but is observed in other images. The bright green starts to appear in 1990 and is located near a water source. In this image, you can see the stream in the lower left corner is also occupied by this bright green vegetation. (more satellite images can be found in the appendix)

Figure 17: Satellite image of the study area modified from Google Earth captured in 2005. Marsh vegetation on the downthrown side of the fault shows a distinct color change. Fault traces for CMWF and CMEF are visible. The browning of the marsh indicates a die-back of the vegetation. Water is beginning to occupy the area. In 2000, more water can be observed on the downthrown side. By 2005, the marsh vegetation seems to repopulate. This is the last year that large swaths of marsh vegetation can be observed. (year 2000 satellite image located in appendix)

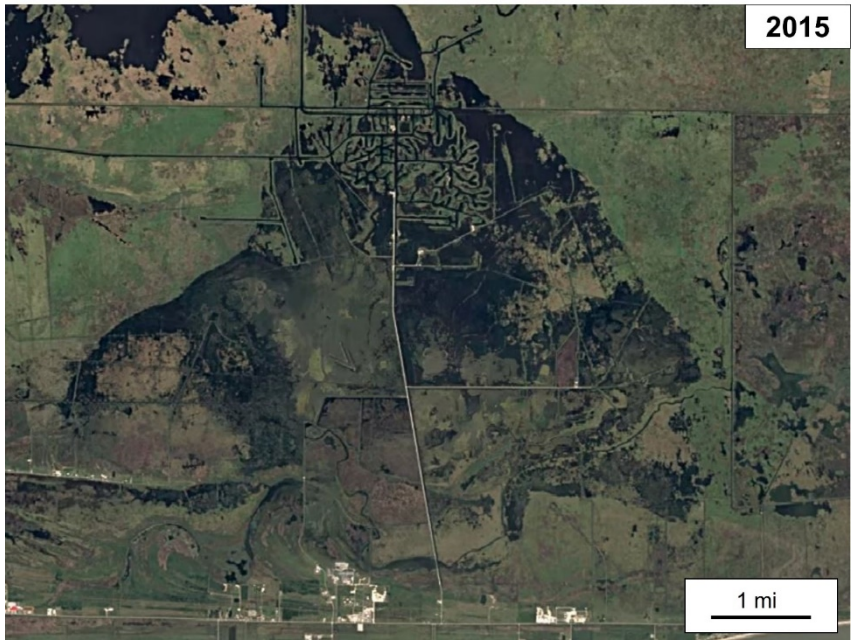

Figure 18: Satellite image of the study area modified from Google Earth captured in 2015. The surface expression of the CMWF and CMEF are clearly visible. A large water body now occupies the downthrown side of the faults. This change occurs rapidly after 2005.

5. Discussion

5.1. Tectonic Land Loss

Land loss is currently one of the recognized threats affecting coastal Louisiana. Controlling factors on land loss in coastal Louisiana are reported to include: (1) reduced sediment flow from the Mississippi River and its tributaries (not considered a factor in this study area), (2) sea-level rise, and (3) subsidence (Chamberlain et al., 2018). In this study, we selected a field area located in the Chenier Plain that is not influenced by the sedimentary processes associated with the Mississippi River. The Chenier Plain is a micro-tidal environment whose limited sediment supply is only dependent on longshore drift currents (Twilley et al., 2016). Sea-level rise is certainly a factor. Southern Louisiana has one of the highest current rates of relative sea-level rise in the world, ranging between 4 and 20 mm/year (Chamberlain et al., 2018). However, the rate of relative sea-level rise is strongly influenced – exacerbated – by subsidence. As previously mentioned, and defined by Yuill et al. (2009), one of the factors leading to subsidence are tectonic processes. The dominant tectonic forces at play along the north coast of the Gulf of Mexico are growth fault activity and halokinesis. These tectonic processes remain understudied, due, in part, to the inaccessibility of industry subsurface data, restricting most subsidence related work to surface data, such as benchmarks, tide gauges, and aerial photographs. Studies conducted by Gagliano et al. (2003) and Dokka (2006), used such data to show subsidence and land loss pattens on downthrown areas of recorded faults. These studies showed downthrown areas of faults breaching the surface would experience land loss as vegetation would die and a water body would occupy its place. Dokka (2006) concluded that a deep-seated component of tectonic origin was possible, due to the velocity data (mm/yr) gathered being inadequate to

explain the subsidence rate where sediment compaction was not a factor. This study investigates the deep-seated tectonic relationship to subsidence and land loss using subsurface data gathered from well logs. Well logs were analyzed to establish fault cuts and map the fault surfaces. The data gathered in the subsurface is compared to surface data acquired from satellite images. From the present-day satellite image, a clear indication of a fault surface trace can be seen outlining either side of the water body. The CMWF fault trace strikes to the NE, with the CMEF fault trace striking to the NW (e.g., Figure 7). Satellite images prior to 1996 show the graben between the faults is occupied by marsh vegetation (Figure 15). However, a discoloration in the graben can be observed as early as 1986 (Figure 15 & 20). A water body now lies in the graben between these fault traces. A documented, and previously mapped, salt dome is positioned between the two faults at the base of the graben. Salt dome halokinesis in the study area initiated the two primary graben faults investigated in this study, and also contributed to the development of many other faults radiating around the salt dome. The graben bounding faults investigated here are the most easily recognized with the technology available to breach the surface and are considered to be the main contributors to subsidence and land loss.

5.2. Characterization of Faults

In an effort to differentiate fault cuts in well logs made by antithetic and synthetic faults, from primary fault cuts, satellite images were integrated to map an artificial/preliminary fault surface using the fault trace as ‘zero feet’ elevation. As mentioned earlier in the Methods section of this paper, a constant dip was used to calculate the spacing of contours on the map surface. The artificial fault surface allowed the author to project a depth range and estimate an intersection with wells to focus the fault cut data search. Stratigraphic correlations above -

2500 ft were difficult and no discernable fault cuts were identified. Some wells were either of poor data quality or not logged deep or shallow enough. Log data at a depth range between -2500 ft and -6000 ft was suitable enough for correlations to be made and fault cuts to be found. The fault surface above the shallowest fault cut depth was extrapolated to the surface using an even contour spacing. The fault cuts found for both the CMWF and CMEF indicate the faults dip steeper than estimated. However, the dip varies not only with depth, but also laterally along the fault surface strike. Both faults are high angle, dipping steeply near the surface and becoming more listric with depth. However, CMWF becomes more listric approaching the top of salt seeming to almost "drape" over the crest of the dome. As previously stated, no evidence of the top of salt was observed from the well logs. The top of salt map interpreted by Sun Oil, as well as the seismic survey accessed through SAI Geoconsulting, Inc., allowed the author to confirm that both CMWF and CMEF truncate at the salt surface. Examination of the mapped fault surfaces and how they relate to the salt, suggest a high probability that the CMWF and CMEF faults are connected. This interpretation establishes a large, singular, highly arcuate fault that strikes E-W across the north flank of the salt dome. The question then, would be whether the faults became connected later, or were established as one at the fault's origin. The decision to map the faults separately is based on the lack of data to confirm a connection.

5.3. Growth Faulting and Stratigraphy

The Middle Miocene horizon mapped using the Amphistegina B paleomarker, does "drape" over the salt dome, with slight thinning observed. Paleo data places the Early Miocene Siphonina Davisi at depths of -5800 to -8000 ft, with the range in depth being affected by salt movement and faulting. The deepest markers are found furthest away from

the salt dome and the shallowest closest to the salt dome. Markers found upthrown of the faults, and not influenced by halokinesis, are found around an average of -6200 ft. The Siphonina Davisi marker found on the down dip flanks of the dome is also slightly thinned. Stratigraphic sequences of large sand sequences, presumably Oligocene in age, are found below the Siphonina Davisi, but are only recognized on the outskirts of the salt dome and are missing on its flanks as well as above. Therefore, salt placement was likely during the Late Oligocene. Diapiric movement, and placement, occurring during the Late Oligocene and Early Miocene, would correlate with other salt diapirs found along the Gulf Coast (Wu et al., 1990). The extension of sediments caused by the salts upward movement resulted in the origination of a graben bounded by the normal faults mapped in this study. An expansion index was calculated indicating a Miocene age for fault growth. Growth was more prevalent in the deeper section, around -5000 ft, with the highest ratio of 1.5. Sections measured around fault cuts located around the -3500 ft range showed slightly less growth, with the highest ratio of expansion being 1.2 (Figures 13 & 14, Tables 1 & 2). It should be noted that no dip data was available. Without dip data in the well section, true stratigraphic thickness is unknown. To gather the best interpretation of general expansion, sections were measured by incorporating large stratigraphic sequences, rather than individual sand or shale packages. Growth can also be seen just below the fault cuts in the hanging wall in some wells. This is possibly due to downward dipping of beds caused by fault growth. Regardless, the expansion index suggests that stratigraphic growth along the fault occurred during the Miocene, as the faults hanging wall actively subsided. If the faults were active during this period, it is reasonable to expect it continue to be active throughout the Quaternary to present day. Furthermore, the evidence for fault activity in the Holocene is supported by land loss in the

hanging wall area (graben) of the mapped faults. The surface characteristics of subsidence due to tectonics in Cameron Meadows Field, are the same characteristics seen across the coast of Louisiana where surface breaching faults are noted. The characteristics of the faults are identifying features that constitute growth faults. This includes the arcuate fault trace observed in map view, a listric fault surface, displacement that increases with depth, and stratigraphic thickening that increases with depth. With a mobile substrate (salt) and growth faults we have a mechanism that tectonically contributes to subsidence that can result in land loss and is not manageable by humans.

Continued fault activity in the Holocene could result from several different factors. The coast of Louisiana rests on the edge of a large passive margin created by the formation of the Gulf of Mexico. Gravitational forces applied on the shelf edge are incessantly influencing movement toward the center of the basin. The study area is known for its oil reserves and presently has active producing wells. Faults are acknowledged as being pathways for the migration of hydrocarbons and other fluids acting as a lubricant facilitating slip along the fault surface. This not only applies to hydrocarbons but to salt brine as well (Cornelio, 2019). If the salt is allochthonous, the detachment of the salt from the feeder stock would accommodate the expansion of sediments in the downthrown section of major growth faults (Wu et al., 1990). Detachment also removes the supporting pressure gradient provided by the feeder stock, which results in further halokinetic processes. All these factors combined can result in the downthrown displacement of the established hanging wall.

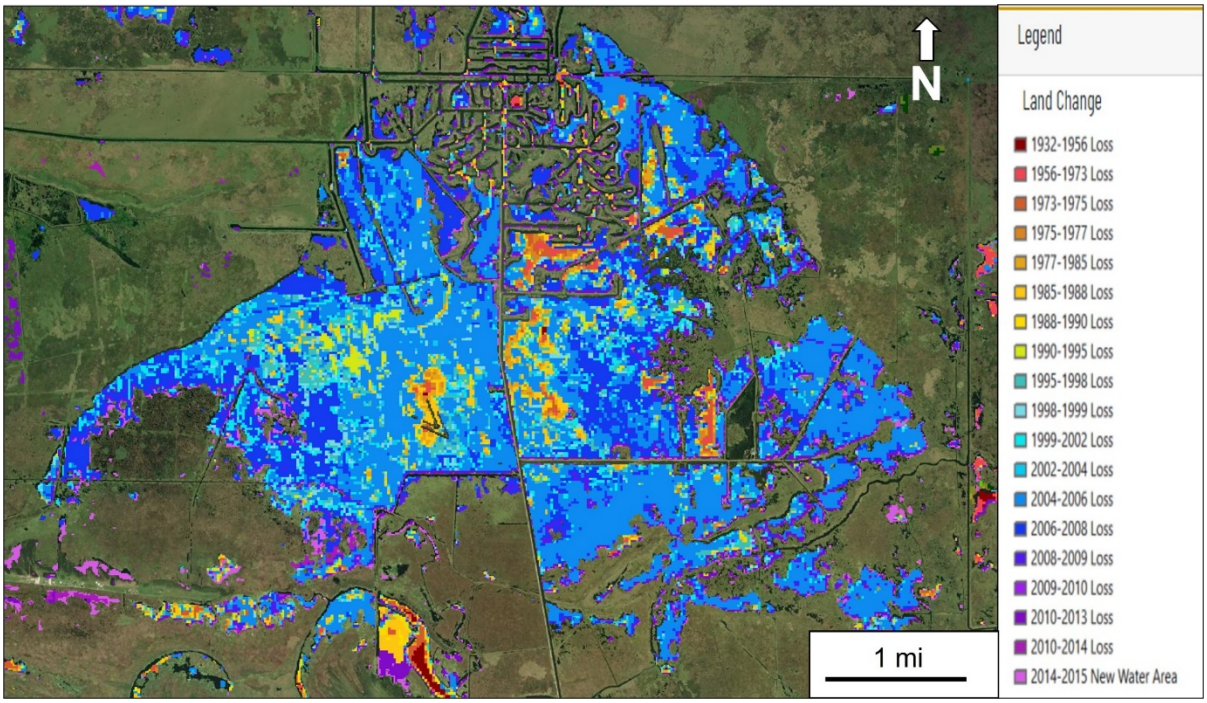

Figure 19: Land change map of study area modified from Louisiana Coastwide Reference Monitoring System (CRMS) and USGS.

6. Conclusion

This study establishes a clear relationship between the deep-seated component of active growth faults and associated halokinesis for subsidence that results in land loss. This study was purposefully conducted in a region of coastal Louisiana not influenced by the processes of the Mississippi deltaic plain to negate any subsidence contributions to land loss attributed to recent sediment deposition compaction. To demonstrate this relationship, a study area in the Chenier Plain of Louisiana experiencing a visible geomorphologic land loss change was chosen. A subsurface investigation using well log data integrated with current and historic satellite images over the study area provide evidence that deep faults breach the surface, and a distinct fault trace can be observed. The fault traces outline a down drop graben structure on top of a shallow salt dome common to the south Louisiana coastal region. This surface fault trace is arcuate in shape and establishes a distinct land change boundary between a waterbody on the downthrown side (in the graben), and thick marsh vegetation on the upthrown side. An expansion index was calculated to determine previous movement along the faults Growth was identified in the hanging wall indicating the fault had become active during the Miocene and suggests potential for the fault to become active again. This potential for future fault activity and deformation is confirmed by historic satellite images.

The historic images show that the area that occupies the hanging wall of the faults, the graben, were once inhabited by lush marsh vegetation. After subsidence, that area is now occupied by a waterbody. This land loss is directly related to the reactivation of growth faults. This relationship is not unique to the study area investigated by this author. The identifying characteristics between fault tectonics and land loss has been documented in other areas of coastal Louisiana, but that documentation is not complete, and the relationship is still

understudied; more data should be collected. Data such as shallow near surface seismic surveys and cores/trenches across fault traces to accurately measure fault displacements and plot rates of change. Dip data in existing wells could lead to a better understanding of recent fault activity in the Holocene but will require intensive subsurface mapping to estimate dip values since these measurements are not routinely collected. The primary goal is to provide insights on how to better protect Louisiana's coastline and infrastructure. This study identifies a geologic mechanism contributing to the loss of coastline that is not controllable by the actions of human society. Understanding this will help us avoid wasting resources on remedies with little to no chance of success. But the process is still not understood.

References

Antonie, J. and W. R. Bryant, 1969, Distribution of salt and salt structure in the Gulf of Mexico: *AAPG Bulletin*, v. 53, p. 2543-2550.

Armstrong, C., Mohrig, D., Hess, T., George, T., & Straub, K. M., 2014, Influence of growth faults on coastal fluvial systems: Examples from the late Miocene to Recent Mississippi River Delta. *Sedimentary Geology*, *301*, 120-132.

Barnes, Stephen R.; Bond, Craig; Burger, Nicholas; Anania, Kate; Strong, Aaron; Weilant, Sarah; and Virgets, Stephanie, 2017, "Economic Evaluation of Coastal Land Loss in Louisiana," *Journal of Ocean and Coastal Economics*: Vol. 4: Iss. 1, Article 3.

Bird, D. E., K. Burke, S. A. Hall, and J. F. Casey, 2005, Gulf of Mexico tectonic history: Hotspot tracks, crustal boundaries, and early salt distribution: *AAPG Bulletin*, v. 89, no. 3, p. 311-328.

Blum, M. D., & Roberts, H. H., 2012, The Mississippi delta region: past, present, and future. *Annual Review of Earth and Planetary Sciences*, *40*, 655-683.

Bornhauser, M., 1958, Gulf Coast tectonics: *American Association of Petroleum Geologists Bulletin*, v. 42, p. 339-370.

Chamberlain, E. L., Törnqvist, T. E., Shen, Z., Mauz, B., & Wallinga, J., 2018, Anatomy of Mississippi Delta growth and its implications for coastal restoration. *Science advances*, 4(4), eaar4740.

Coleman, J. M., Roberts, H. H., & Gregory W. Stone., 1998, Mississippi River Delta: An Overview. *Journal of Coastal Research*, *14*(3), 699–716. http://www.jstor.org/stable/4298830

Cornelio, C., Spagnuolo, E., Di Toro, G., Nielsen, S., & Violay, M., 2019, Mechanical behaviour of fluid-lubricated faults. *Nature communications*, *10*(1), 1-7.

Couvillion, B.R., Beck, Holly, Schoolmaster, Donald, and Fischer, Michelle, 2017, Land area change in coastal Louisiana 1932 to 2016: U.S. Geological Survey Scientific Investigations Map 3381, 16 p. pamphlet.

Culpepper, D.; McDade, E.; Dawers, N.; Kulp, M., and Zhang, R., 2019, Synthesis of fault traces in SE Louisiana relative to infrastructure. Tran-SET Project No. 17GTLSU12. Publications, 30.

Day, J. W. Jr et al., 2007, Restoration of the Mississippi Delta: Lessons from Hurricanes Katrina and Rita. *Science 315*, 1679–1684.

Dokka, R. K., 2006, Modern-day tectonic subsidence in coastal Louisiana, Geology, v. 34, p. 281–284.

Dokka, R. K., Sella, G. F., and Dixon, T. H., 2006, Tectonic control of subsidence and southward displacement of southeast Louisiana with respect to stable North America, *Geophys. Res. Lett.*, 33.

Fisk, H. N., and E. McFarlan, Jr., 1955, Late Quaternary deltaic deposits of the Mississippi River: *Geol. Soc. America Special Paper* Vol. 62, p. 297-302.

Frederick, B. C., Blum, M., Fillon, R., & Roberts, H., 2019, Resolving the contributing factors to Mississippi Delta subsidence: Past and Present. *Basin Research*, *31*(1), 171-190.

Gagliano, S.M., Kemp, E.B.,Wicker, K.M., Wiltenmuth, K.S., Sabate, R.W., 2003, Neo-tectonic Framework of Southeast Louisiana and Applications to Coastal Restoration: *Gulf Coast Association of Geological Societies*, v. 53, pp. 262-272.

Gonzalez, Juan & Törnqvist, Torbjörn., 2006, Coastal Louisiana in crisis: Subsidence or sea level rise?. *Eos Transactions American Geophysical Union*. 87. 493, 498.

Google Earth 9.159.0.0. 1985-2022, Cameron Parish, LA, USA. 29° 49' 43"N, 93° 38' 00"W, Camera alt 20 km. Data SIO, NOAA, U.S. Navy, NGA, GEBCO. (Accessed April 20, 2022).

Howe, H.V., R.J. Russell, and J.H. McGuirt., 1935, Physiography of coastal southwest Louisiana: *Louisiana Geological Survey Bulletin*, v. 6, p. 1–68.

Howe, H. V., R. J. Russell, J. H. McGuirt, B. C. Craft, and M. B. Stephenson, 1935, Reports on the Geology of Cameron and Vermilion Parishes: *New Orleans Department of Conservation, Louisiana Geological Survey, Geological Bulletin* 6.

Hoyt, J. H., 1969, Chenier Versus Barrier, Genetic and Stratigraphic Distinction, *American Association of Petroleum Geologists Bulletin*. v. 53, No. 2, p. 299-305.

Hudec, M. R., Norton, I. O., Jackson, M. P., & Peel, F. J., 2013, Jurassic evolution of the Gulf of Mexico salt basin. *AAPG bulletin*, *97*(10), 1683-1710.

Jankowski, K. L., Törnqvist, T. E., & Fernandes, A. M., 2017, Vulnerability of Louisiana's coastal wetlands to present-day rates of relative sea-level rise. *Nature Communications*, 8, 14792.

Kuecher, G. J., 1995, The dominant processes responsible for subsidence of coastal wetlands in south Louisiana, in Land Subsidence: *Proceedings of the Fifth International Symposium on Land Subsidence*, edited by F. J. Barends et al., pp. 69–81, Int. Assoc. of Hydrol. Sci., The Hague, Netherlands.

Kuecher, G. J., Roberts, H. H., Thompson, M. D., & Matthews, I., 2001, Evidence for active growth faulting in the Terrebonne delta plain, south Louisiana: Implications for wetland loss and the

vertical migration of petroleum. *Environmental Geosciences*, *8*(2), 77-94.

Kulp, M.A., 2000. *Holocene Stratigraphy, History, and Subsidence of the Mississippi River Delta Region, North-Central Gulf of Mexico. Lexington, Kentucky*: University of Kentucky, Master's thesis, 336p.

Martin, R. G., 1978, Northern and eastern Gulf of Mexico continental margin: stratigraphic and structural framework: *AAPG Studies in Geology* No. 7, p. 21-42.

Meckel, T.A., Ten Brink, U.S. and Williams, S.J., 2007, Sediment compaction rates and subsidence in deltaic plains: numerical constraints and stratigraphic influences. Basin Research, 19: 19-31.

Nienhuis, J. H., Tornqvist, T. E., Jankowski, K. L., Fernandes, A. M., and Keogh, M. E., 2017, A new subsidence map for coastal Louisiana. *GSA Today*, 27, 58-59.

O'Leary, M. C. 2018, Relationship between Growth Faults and Subsidence: Impact on Coastal Erosion, an Example from Cameron Parish, Southwestern Louisiana, USA. University of Louisiana at Lafayette.

O'Leary, M., & Gottardi, R. 2020, Relationship between growth faults, subsidence, and land loss: An example from Cameron Parish, Southwestern Louisiana, USA. *Journal of Coastal Research*, *36*(4), 812-827.

Owen, D.E., 2008, Geology of the Chenier Plain of Cameron Parish, southwestern Louisiana: *Geological Society of America Field Guide* 14, 2008 Joint Annual Meeting, Houston, Texas, 5–9 October 2008, p. 27–38.

Penland, S., and J. R. Suter, 1989, The Geomorphology of the Mississippi River chenier plain: *Marine Geology*, v. 90, p. 231-258.

Reed, J. M. 1994, Probable Cretaceous-To-Recent Rifting in The Gulf Of Mexico Basin An answer to Callovian salt deformation and distribution problems? Part 1. *Journal of Petroleum Geology*, *17*(4), 429-444.

Rowan, M. G., Jackson, M. P., & Trudgill, B. D. (1999). Salt-related fault families and fault welds in the northern Gulf of Mexico. *AAPG bulletin*, *83*(9), 1454-1484.

Russell, R.J., and H.V. Howe., 1935, Cheniers of southwestern Louisiana: *Geographical Review*, v. 25, p. 449–461.

Salvador, A., 1987, Late Triassic-Jurassic Paleogeography and Origin of Gulf of Mexico Basin: *The American Association of Petroleum Geologists Bulletin*, v. 71, no. 4, p. 419–451.

Shen, Z., Dawers, N.H., Törnqvist, T.E., Gasparini, N.M., Hijma, M.P. and Mauz, B., 2017, Mechanisms of late Quaternary fault throw-rate variability along the north central Gulf of Mexico coast: implications for coastal subsidence. Basin Res, 29: 557-570.

Tearpock, D. J., and R. E. Bischke, 1991, Applied subsurface geological mapping, p. 256 - 264.

Törnqvist, T. E., Bick, S. J., van der Borg, K., & de Jong, A. F. (2006). How stable is the Mississippi Delta? *Geology*, *34*(8), 697-700.

Törnqvist, T., Wallace, D., Storms, J. *et al.,* 2008, Mississippi Delta subsidence primarily caused by compaction of Holocene strata. *Nature Geosci* **1,** 173–176.

Twilley, Robert R. et al. "Co-evolution of wetland landscapes, flooding, and human settlement in the Mississippi River Delta Plain." 26 May 2016.

Worrall, D.M., and S. Snelson, 1989, Evolution of the northern Gulf of Mexico, in Bally, A.W., and Palmer A.R., eds., The Geology of North America—An overview, Boulder, Colorado, Geological Society of America, Geology of North America, v. A, pp. 97-138.

Wilhelm, O., & Ewing, M., 1972, Geology and history of the Gulf of Mexico. *Geological Society of America Bulletin*, *83*(3), 575-600.

Wolstencroft, M., Shen, Z., Törnqvist, T. E., Milne, G. A., & Kulp, M., 2014, Understanding subsidence in the Mississippi Delta region due to sediment, ice, and ocean loading: Insights from geophysical modeling. *Journal of Geophysical Research: Solid Earth*, *119*(4), 3838-3856.

Wu, S., Bally, A., and Cramez, C., 1990, Allochthonous salt, structure and stratigraphy of the north-eastern Gulf of Mexico. Part 2: Structure. *Marine and Petroleum Geology*,1990, Vol 7, Nov. p 334-370.

Yu, S. Y., Törnqvist, T. E., & Hu, P., 2012, Quantifying Holocene lithospheric subsidence rates underneath the Mississippi Delta. *Earth and Planetary Science Letters*, *331*, 21-30.

Yuill, B.; Lavoie, D., and Reed, D.J., 2009, Understanding subsidence processes in coastal Louisiana. In: FitzGerald, D. and Reed, D.J. (eds.), Geologic and Environmental Dynamics of the Pontchartrain Basin. *Journal of Coastal Research, Special Issue* 54, pp. 23–36.

Biographical Sketch

Wiley Melvin Griffin IV was born and raised in Bainbridge, Georgia on May 1st, 1991. He is the son of Wiley M. Griffin III and the late Cynthia P. Griffin. He attended Bainbridge High School and graduated with honors in 2009. Following a brief career in law enforcement, he attended Valdosta State University graduating with a Bachelor of Science in geology in 2019. During his time at Valdosta State, he was a member of Sigma Nu fraternity serving on the executive board as Marshal from 2016-2017 and was also a member of the VSU Geological Student Society, serving on the executive board as Secretary from 2018-2019. After receiving his bachelors, he enrolled in the graduate school of University of Louisiana at Lafayette, graduating with a Master of Science in geology in the Summer of 2022. During his time at UL Lafayette, he served as the student chapter's AAPG President from 2021-2022 and sat on the Lafayette Geological Society board as a Student Liaison during that same year.